

Perceptually Constrained Adversarial Attacks

Muhammad Zaid Hameed¹, András György²

¹Department of Computing, Imperial College London, UK

²DeepMind, London, UK

Email: muhammad.hameed13@imperial.ac.uk, agyorgy@google.com

Abstract

Motivated by previous observations that the usually applied L_p norms ($p = 1, 2, \infty$) do not capture the perceptual quality of adversarial examples in image classification, we propose to replace these norms with the structural similarity index (SSIM) measure, which was developed originally to measure the perceptual similarity of images. Through extensive experiments with adversarially trained classifiers for MNIST and CIFAR-10, we demonstrate that our SSIM-constrained adversarial attacks can break state-of-the-art adversarially trained classifiers and achieve similar or larger success rate than the elastic net attack, while consistently providing adversarial images of better perceptual quality. Utilizing SSIM to automatically identify and disallow adversarial images of low quality, we evaluate the performance of several defense schemes in a perceptually much more meaningful way than was done previously in the literature.

1 Introduction

In recent years, the advances in machine learning have enabled solving problems in artificial intelligence, such as understanding speech, natural languages, or images, at an unprecedented accuracy, enabling such systems being deployed in practical applications. This growing use of machine learning methods has given rise to concerns about their security and reliability, especially for one of the most practical methods, known as deep learning (DL). In particular, it has been demonstrated that modifications to their input (e.g., an image or speech signal), imperceptible to humans, can fool deep learning models and make them commit unexpected errors. These modifications are known as adversarial attacks or adversarial input perturbations [Goodfellow et al., 2015, Kurakin et al., 2017, Chen et al., 2018, Carlini and Wagner, 2017].

Specifically, in image classification the goal of adversarial attacks is to fool a classifier such that the created adversarial images have similar high-level features as the original inputs, so that for a human oracle they belong to the same class (a stricter version of this requirement is that the difference of the original and the adversarial images should be imperceptible for a human oracle). On the other hand, in practice, in most cases the quality of the adversarial perturbations is measured through pixelwise distortion measures in some L_p distance (with $p \in \{1, 2, \infty\}$), operationalizing the assumption that if two images have small distance in these distortion measures than they are perceptually similar, that is, they have similar high-level features. At the same time, Sharif et al. [2018] demonstrated that having a small L_p distance is both unnecessary and insufficient for perceptual similarity and proposed the use of other similarity measures available in the literature [Wang et al., 2004, Wang and Bovik, 2002, Yee et al., 2001] which are more aligned with human perception. Sharif et al. [2018] also showed that these perception-based similarity measures are not fully satisfactory either, for example, they cannot handle geometric transformations such as rotations or translations, and carefully introducing patches from other images might produce significantly different values for perceptual similarity measures.

A direct implication of this result is that the adversarial attacks using pixelwise L_p -distances as a proxy for perceptual similarity may produce adversarial images which will be near in L_p -distance to the original images, but either belong to some other class or are destroyed beyond recognition. Figure 1 shows such a case when two adversarial attacks produce successful adversarial images with almost equal L_p -distances from the original image (simultaneously for $p = 1, 2, \infty$), but one of the images (obtained by the state-of-the-art elastic net attack of Chen et al. 2018) is nearly

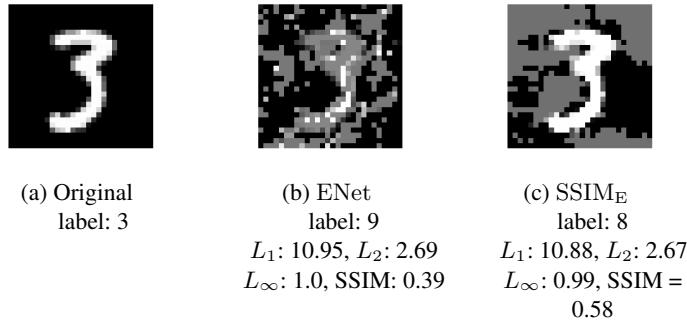


Figure 1: L_p distances do not convey significant information about perceptual similarity between images. Subfigures (a), (b), (c), respectively, show an original MNIST digit, an adversarial version created by the elastic net (ENet) attack and our SSIM-based SSIM_E attack. Class labels given by the classifier, L_p distances for $p \in \{1, 2, \infty\}$, and SSIM are also shown.

destroyed beyond recognition, while the other adversarial image (created by one of our proposed attacks based on perceptual similarity) could be easily classified by a human oracle. At the same time, defense strategies which use the same underlying assumption that images close in some L_p -distance belong to the same class suffer from the fact that they try to assign the same class label to different images with small L_p -distances, instead of being perceptually similar. Thus, adversarial images which are not near in some L_p -distance but share the same high-level features can potentially break these defense methods.

In order to alleviate these shortcomings of current adversarial attack and defense approaches, we explore perceptual similarity in determining the quality of adversarial attacks and the robustness of defense strategies against these attacks. More specifically, our contributions in this work are as follows:

- We propose to use the structural similarity index (SSIM) measure [Wang et al., 2004] as a quality metric for perceptual similarity of adversarial images and show that SSIM is quite effective in quickly and automatically finding adversarial images of low quality, for example, when an attack destroys the whole image.
- We propose SSIM-based adversarial attacks, and show that they are able to break state-of-the-art defense schemes, achieving similar or larger success rate than the state-of-the-art elastic net attack (ENet) [Chen et al., 2018] (and also much stronger than the simple L_∞ -constrained projected gradient descent, PGD, attack [Madry et al., 2018]), while consistently producing adversarial images of better perceptual quality.

1.1 Related Work

Adversarial examples were first discovered by Bruna et al. [2014], who found that for state-of-the-art CNN-based image classifiers, for almost all images it is possible to create a perturbation with a small L_2 norm such that when added to the input image, it changes the class label predicted by the classifier while the resulting input image is visually similar to the original input image. Since then a multitude of schemes were suggested to create such adversarial perturbations, mostly for classification; the most popular class of these methods phrases the task as a constrained optimization problem in the input space, where the error (and often the confidence in the prediction) of the classifier is maximized over the set of inputs which are close to the original input in some L_p distances [Goodfellow et al., 2015, Kurakin et al., 2017, Madry et al., 2018, Papernot *et al.*, 2017, Tramèr et al., 2018, Carlini and Wagner, 2017, Chen et al., 2018, Rony et al., 2019].

In parallel, several defense methods were developed to train classifiers which are more robust to such adversarial perturbations. Most of these schemes use some form of adversarial training, which uses carefully created adversarial examples during the training of a classifier Huang et al. [2015], Madry et al. [2018], Yan et al. [2018], Goyal et al. [2018], Shafahi et al. [2019], Rony et al. [2019]. Following the same principles, Zhang and Wang [2019] introduced perturbations by constraining the changes in the feature space instead of the input space, further increasing the performance of these attacks.¹ Yet, this defense scheme can also be broken, e.g., with the elastic net attack [Chen et al.,

¹These methods can be combined with other approaches, such as using ensembles for classifiers [Cohen et al., 2019] or using unlabelled data in

2018], however, in such successful attacks the images are often heavily distorted and sometimes even destroyed beyond recognition.

In this work we address this problem by constraining adversarial perturbations using perceptual similarity measures, namely SSIM [Wang et al., 2004], and show that even the best defense schemes (to date) can be (almost) completely broken by visually acceptable adversarial images. Two recent papers [Gragnaniello et al., 2019, Zhao et al., 2020], developed in parallel of our work (one of them only published on arXiv), also use perceptual distance measures: Gragnaniello et al. [2019] proposed to use SSIM to create adversarial examples, while Zhao et al. [2020] used the perceptual color distance for the same purpose. Both works demonstrate that their proposed attack method works well against standard classifiers with simple defense schemes, such as JPEG compression [Dziugaite et al., 2016], bit-depth reduction [Xu et al., 2018, Guo et al., 2018], or nearest neighbor classification. Since such classifiers are easily broken even by L_p -constrained attacks (such as PGD by Madry et al. 2018 or ENet by Chen et al. 2018) while introducing little visual artifacts, the evaluation of these attacks is limited. In contrast, we study the performance of our attack methods against adversarially trained networks, which is a much more challenging task [Athalye et al., 2018], and show that the attacks are able to break even state-of-the-art defense schemes while producing high-quality adversarial images.

2 Perceptually Constrained Adversarial Attacks

We consider a score-based classifier of inputs $x \in \mathbb{R}^n$ to a set of labels $\mathcal{S} = \{1, 2, \dots, S\}$, defined by the score function $f : \mathbb{R}^n \times \mathcal{S} \rightarrow \mathbb{R}$, assigning a label $\hat{s} \in \arg \max_{s \in \mathcal{S}} f(x, s)$ to x . With a slight abuse of notation, throughout we also use f to denote the classifier, $f(x)$ to denote the label assigned to x , and $f_s(x) = f(x, s)$ to denote the score of class s .

Let x be an image correctly classified by f , that is, $s = f(x)$, the true label. An adversarial attack on this classifier f aims to modify the input image x with a perturbation $\delta \in \mathbb{R}^n$, such that $f(x + \delta) \neq f(x)$, that is, the class label is changed from the original correct prediction. Since x is correctly classified, $f_s(x) - \max_{s' \neq s} (f_{s'}(x)) > 0$, and δ is a successful adversarial perturbation if the class label changes, that is, $f_s(x + \delta) - \max_{s' \neq s} (f_{s'}(x + \delta)) < 0$. To find such a δ , following Carlini and Wagner [2017], we minimize a loss function $\ell(x, \delta)$ defined such that $\ell(x, \delta) = 0$ only when this condition is met:

$$\ell(x, \delta) = c \left(f_s(x + \delta) - \max_{s' \neq s} f_{s'}(x + \delta) + \mathcal{K} \right)^+, \quad (1)$$

where \mathcal{K} represents some required margin, $c > 0$ is a scaling factor (the role of c will be to balance the loss function and the additional regularization terms in Eq. 2) and a^+ is a short-hand for $\max(a, 0)$ (note that $\ell(x, \delta)$ depends on x and δ through their sum $x + \delta$ and the true label s of x). A solution of the resulting unconstrained optimization problem $\arg \min_{\delta} \ell(x, \delta)$ is an adversarial example with a score-margin of at least \mathcal{K} when $\ell(x, \delta) = 0$. To keep the resulting image $x + \delta$ close to x , the attack methods in the literature use a constrained formulation requiring that some similarity measure $Q(x, x + \delta)$ between the input x and its perturbed version $x + \delta$ is lower bounded by some value ζ , leading to the optimization problem

$$\arg \min_{\delta} \ell(x, \delta) \text{ such that } Q(x, x + \delta) \geq \zeta. \quad (2)$$

In the literature, Q is some negative L_p distance, that is, $Q(x, x + \delta) = -\|\delta\|_p$ with $p \in \{1, 2, \infty\}$ usually, and instead of the constrained optimization formalization (2), a Lagrangian formulation

$$\arg \min_{\delta} \ell(x, \delta) + \lambda(\zeta - Q(x, x + \delta)) \quad (3)$$

is used with some $\lambda > 0$ [Goodfellow et al., 2015, Kurakin et al., 2017, Chen et al., 2018, Carlini and Wagner, 2017].

As the similarity measure Q , we consider the structural similarity index (SSIM) measure [Wang et al., 2004] defined, for gray-scale images $x, y \in \mathbb{R}^n$, as

$$\text{SSIM}(x, y) = [l(x, y)]^\alpha \cdot [c(x, y)]^\xi \cdot [s(x, y)]^\gamma, \quad (4)$$

the training [Carmon et al., 2019], but looking at such combinations is orthogonal to the questions we consider here and, hence, are out of the scope of the paper.

where $l(x, y) = \frac{2\mu_x\mu_y + C_1}{\mu_x^2 + \mu_y^2 + C_1}$ is luminance with μ_x and μ_y denoting the mean pixel value of x and y , resp., $c(x, y) = \frac{2\sigma_x\sigma_y + C_2}{\sigma_x^2 + \sigma_y^2 + C_2}$ is the contrast function with σ_x and σ_y denoting the standard deviation of pixel values of x and y , resp., and $s(x, y) = \frac{\text{cov}_{xy} + C_3}{\sigma_x\sigma_y + C_3}$ is the structure comparison function with cov_{xy} denoting the pixelwise covariance between images x and y ; here $C_1, C_2, C_3 > 0$ and $\alpha, \xi, \gamma > 0$ are appropriate constants. In case of RGB images, the SSIM is calculated for each channel and then the average SSIM value across the different color channels is computed. For $\alpha = \xi = \gamma = 1$ and $C_3 = \frac{C_2}{2}$, (4) simplifies to

$$\text{SSIM}(x, y) = \underbrace{\frac{2\mu_x\mu_y + C_1}{\mu_x^2 + \mu_y^2 + C_1}}_{S_1} \cdot \underbrace{\frac{2\text{cov}_{xy} + C_2}{\sigma_x^2 + \sigma_y^2 + C_2}}_{S_2}. \quad (5)$$

We use the same values for all parameters (C_1, C_2, C_3) as Wang et al. [2004] (specifically, $\sqrt{C_1}$ and $\sqrt{C_2}$ are 0.01, resp., 0.03 times the range of the coordinates of x). To compute the adversarial attack, we would like to solve the optimization problem (3) with $Q = \text{SSIM}$. The non-cocavity of SSIM makes this optimization problem hard (even though f is non-convex by itself, this is an issue in practice). Therefore, following Brunet et al. [2011], we aim to optimize separately the two terms $S_1 = S_1(\mu_x, \mu_y)$ and $S_2 = S_2(x - \mu_x, y - \mu_y)$ in (5), where, with a slight abuse of notation, $x - \mu_x$ denotes an n -dimensional vector with its i th coordinate being defined as $x_i - \mu_x$ (and $y - \mu_y$ is defined similarly). The benefit of this approach is that $-S_1$ and $-S_2$ can be shown to be quasi-convex (i.e., all their level sets are convex) [Brunet et al., 2011]: Consider the normalized mean squared error (NMSE) function $\text{NMSE}(u, v, C) = \frac{\|u-v\|^2}{\|u\|^2 + \|v\|^2 + C}$ for $u, v \in \mathbb{R}^d$ and $C \geq 0$ which is quasi-convex in u on the set $\{u : \langle u, v \rangle \geq -C/2\}$ for a fixed v . Then we have

$$\begin{aligned} S_1(\mu_x, \mu_y) &= 1 - \text{NMSE}(\mu_x, \mu_y, C_1), \\ S_2(x - \mu_x, y - \mu_y) &= 1 - \text{NMSE}(x - \mu_x, y - \mu_y, C_2), \end{aligned}$$

showing quasi-convexity for the appropriate regions for x for a fixed y : $-S_1$ is quasi convex on $P_1 = \{x : \mu_x\mu_y \geq -\frac{C_1}{2}\}$ and $-S_2$ is quasi-convex on $P_2 = \{x - \mu_x : \langle x - \mu_x, y - \mu_y \rangle \geq -\frac{C_2}{2}\}$.

Now, to simplify the minimization process, instead of the constraint $\text{SSIM}(x, y) \geq \zeta$, we consider $S_1 \geq \zeta_1$ on P_1 and $S_2 \geq \zeta_2$ on P_2 . Ensuring the lower bounds on S_1 and S_2 and that the adversarial image falls into $P_1 \cap P_2$, we have the constraints

$$\begin{aligned} g_1(y, x) &= \zeta_1 - \left(1 - \frac{(\mu_x - \mu_y)^2}{\mu_x^2 + \mu_y^2 + C_1}\right) \leq 0; \\ g_2(y, x) &= \zeta_2 - \left(1 - \frac{\|(x - \mu_x) - (y - \mu_y)\|^2}{\|(x - \mu_x)\|^2 + \|y - \mu_y\|^2 + C_2}\right) \leq 0; \\ g_3(y, x) &= -2\mu_x\mu_y - C_1 \leq 0; \\ g_4(y, x) &= -2\langle x - \mu_x, y - \mu_y \rangle - C_2 \leq 0. \end{aligned}$$

Note that for $[0, 1]$ -valued pixels, $g_3(y, x) \leq 0$ always holds with our choice of C_1 . To minimize $\ell(x, \delta)$ subject to the constraints above, we formulate the Lagrangian

$$L(\delta, \boldsymbol{\lambda}) = \ell(x, \delta) + \sum_{i=1}^4 \lambda_i g_i(x + \delta, x), \quad (6)$$

which is a relaxed version of (3) (here $\boldsymbol{\lambda} = (\lambda_1, \dots, \lambda_4)$), and simultaneously minimize it over δ and maximize it in the Lagrangian multipliers $\boldsymbol{\lambda}$, similarly to Cotter et al. [2019]. The resulting gradient-based (first-order) optimization method is presented in Algorithm 1, where to make an update in δ and $\boldsymbol{\lambda}$, we use first-order optimization algorithms A_δ and A_λ , where $A_i(x, \nabla_x)$ provides the next iteration from x using gradient ∇_x . In practice, these algorithm can be chosen, e.g., as gradient descent or Adam [Kingma and Ba, 2015] (e.g., when A_δ is the gradient descent algorithm, $A_\delta(\delta^t, \nabla_\delta L(\delta^t, \boldsymbol{\lambda}^t)) = \delta^t - \eta \nabla_\delta L(\delta^t, \boldsymbol{\lambda}^t)$ for some step size $\eta > 0$). Of course, since our optimization problem is non-convex, Algorithm 1 is not guaranteed to find the solution of the constrained minimization problem.

While in Algorithm 1 we initialize δ and $\boldsymbol{\lambda}$ with zero, in practice it is often beneficial to start from a reasonably good local optimum. For this reason, we also consider starting the optimization from the perturbation given by the

Algorithm 1 Optimization of the Lagrangian (6).

Input: $T \in \mathbb{N}$, iterative gradient-based optimization algorithms A_δ and A_λ
Initialize: $\delta^1 = 0, \lambda^1 = 0$
for $t = 1, \dots, T$ **do**
 Update $\hat{\delta}^{t+1} = A_\delta(\delta^t, \nabla_\delta L(\delta^t, \lambda^t))$
 Update $\delta^{t+1} = \text{clip}(x + \hat{\delta}^{t+1}, [0, 1]^n) - x$
 Update $\lambda^{t+1} = \max\{A_\lambda(\lambda^t, -\nabla_\lambda L(\delta^t, \lambda^t)), 0\}$
end for
Return $x + \delta^T$

elastic net (ENet) attack [Chen et al., 2018], obtained as the (approximate) solution of the loss minimization with an elastic loss penalty:

$$\delta^* = \arg \min_{x+\delta \in [0,1]^n} \ell(x, \delta) + \beta \|\delta\|_1 + \|\delta\|_2^2 \quad (7)$$

for some $\beta > 0$. Note that this is a special case of (3) with $Q(x, x + \delta) = -\beta \|\delta\|_1 - \|\delta\|_2^2$. Our ENet-initialized attack can be interpreted as an SSIM-based perceptual improvement over the ENet attack. In the ENet attack, Chen et al. [2018] proposed to optimize the elastic-loss objective (7) by some first-order optimization algorithm, augmented with a binary search over the parameter c , used in the definition of the loss function (see Algorithm 2 in the appendix), which we also adopt in computing our attacks.

3 Experimental Evaluation

In this section we present experiments showing the effectiveness of our SSIM-based attacks. Unlike concurrent work [Gragnaniello et al., 2019, Zhao et al., 2020], we consider adversarially trained networks for both the MNIST [LeCun and Cortes, 2010] and the CIFAR-10 [Krizhevsky, 2009] datasets. We compare our attack methods to standard and state-of-the-art adversarial attacks: the elastic net attack (ENet) [Chen et al., 2018] given in (7), which aims to obtain adversarial images with perturbations of small L_1 - and L_2 -norms, and the projected gradient descent attack (PGD) in L_∞ -norm [Madry et al., 2018].

The basic version of the SSIM attack (initialized at zero) is denoted by SSIM, while the one which is initialized at the ENet attack is denoted by SSIM_E. In the implementation (Algorithm 1), we used gradient descent as A_δ and the Adam optimizer [Kingma and Ba, 2015] as A_λ , as this combination led to the most successful adversarial perturbations with large SSIM values. To properly tune the scaling coefficient c in (1), we use binary search, as proposed by [Chen et al., 2018] for the ENet attack (details are given in Algorithm 2 in the appendix); the same method is used in ENet. In SSIM_E, we use the same c in the optimization as the one obtained by ENet during the initialization.

In the experiments we set the confidence \mathcal{K} to 0 in the loss function (1). ENet was implemented with $\beta = 0.01$. We used 9 binary search steps, each of which involved 1000 iterations each with initial learning rate 0.01 reduced with the square-root of the number of iterations.

For MNIST we analyze the performance of these attacks for a single classifier, while for CIFAR-10 we consider three defense schemes.

3.1 SSIM Attack on MNIST

For the MNIST dataset (with pixel intensities scaled to $[0, 1]$), we compare the performance of the attack methods against an adversarially trained network. We use a convolutional neural network from the Cleverhans library [Papernot et al., 2018] with three convolution layers of 64, 128 and 256 filters (of size 3×3), respectively, with ReLU activations and one fully connected layer of size 128. Following Madry et al. [2018], the network was trained with a mix of clean and adversarial images generated by 20 iterations of the PGD attack with maximum L_∞ -perturbation $\epsilon = 0.3$. Figure 2 shows the performance of the adversarial attacks used for comparison in terms of attack success, average SSIM value and L_p distortions for $p \in \{1, 2, \infty\}$ for successful adversarial images.

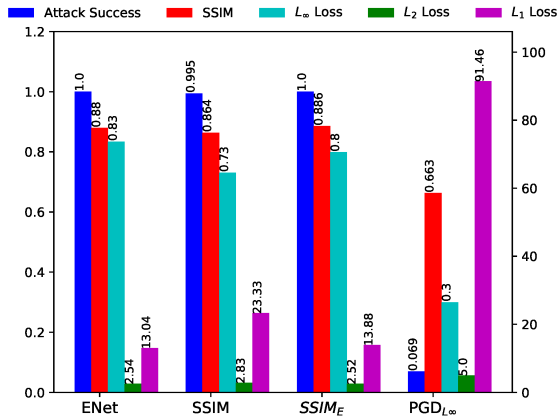


Figure 2: Performance of adversarial attacks on MNIST with adversarial training.

The PGD attack was tested with the same parameters as the ones used for generating adversarial images during adversarial training. It can be seen that the adversarial training indeed helped, and the attack succeeded on the test data only in 7% of the images. On the other hand, the other three attacks, ENet, SSIM and SSIM_E achieve 100% (or almost 100% for SSIM) success rate. We analyze the quality of these attacks using the SSIM values of the adversarial images. First we use SSIM to find the most distorted images; this is shown in Figure 3 for the ENet and SSIM attacks. The figure shows the images for which ENet, resp. SSIM, produce adversarial images with the lowest SSIM values, together with the adversarial attacks generated by the other methods for the same images. The SSIM values and the perceived labels are shown for each image (on top and on the left hand side, resp.), and red frames indicate if an attack is successful, that is, the resulting image is misclassified.

It can be seen that the adversarial images generated using the ENet attack with the smallest SSIM values are destroyed to an extent that they have become unrecognizable. On the other hand, for the same images, the SSIM attack generates successful adversarial images which have relatively higher SSIM values and can be easily recognized by a human oracle. SSIM_E also improves quite a lot over the images generated by ENet. Taking a closer look at digit 3 in Figure 3 (a), shown in Figure 1 together with L_p -distortion and SSIM values, one can see the positive effect of SSIM_E over ENet, as the images produced by the two attacks have almost identical L_1 , L_2 , and L_∞ distances from the original, but the SSIM value of the image produced by SSIM_E is much higher and the digit is easy to recognize for a human oracle, unlike the one produced by the ENet attack. These (and several other similar) images) raise serious concerns not only about the 100% success rate of the ENet attack or other adversarial attacks proposed in literature, and support the observations of Sharif et al. [2018] about the unsuitability of L_p -distances to assess the quality of adversarial images. Note that here the SSIM_E attack produces images with better perceptual quality compared to both ENet and SSIM attacks, while the PGD attack is unsuccessful on these, supposedly hard-to-perturb, images.

In order to further evaluate the performance of different adversarial attacks in terms of the SSIM values of successful adversarial examples, we show the success rate of different adversarial attacks as a function of SSIM values in Figure 4 (a). It can be seen that for the proposed SSIM and SSIM_E attacks, even the worst case SSIM value is above 0.5, which is significantly higher than both for the ENet and PGD attacks. In the bottom part of figure (a), we show for each attack the proportion of the adversarial images above a certain SSIM value (the *tail probability*). As almost all adversarial images generated by ENet, SSIM, and SSIM_E are successful, the success rate at a given SSIM level is approximately the same as the tail probability. The three attacks are equally good when the requirement is to achieve a minimum SSIM value up to 0.8, which guarantees high-quality images, as shown in Figure 4 (b); notably, the success rate of the attacks requiring this minimum SSIM value is above 80%. For higher minimum SSIM values, ENet becomes somewhat better than SSIM, although SSIM_E remains the best. The produced images are also of high quality, as demonstrated in Figure 4 (b), showing some images with SSIM around and above 0.8, where the attacks achieve over 80% success rate. On the other hand, PGD is much less effective, e.g., the 30% of samples distorted below an SSIM value of 0.6 only result in a few percent success in generating adversarial images. PGD also produces images with low SSIM value in general (e.g., the highest value achieved is approximately 0.9).

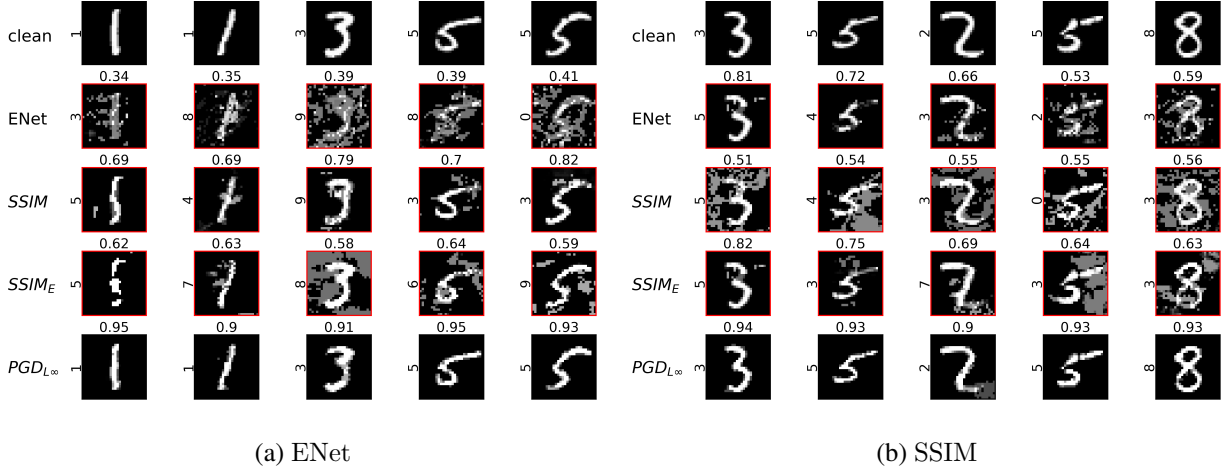


Figure 3: Adversarial images for the ENet and the SSIM attacks with smallest SSIM values on the MNIST dataset.

DEFENSE	CLEAN	$\epsilon = \frac{8}{255}$	$\epsilon = \frac{12}{255}$	$\epsilon = \frac{16}{255}$	$\epsilon = \frac{20}{255}$
Madry _{xent}	87.25	45.86	28.68	19.69	14.46
Madry _{CW}	87.25	47.01	30.22	20.41	14.53
Free _{xent}	86.05	47.04	27.52	15.63	8.39
Free _{CW}	86.05	47.23	28.31	16.24	8.7
Feature _{xent}	89.98	70.81	67.52	64.64	61.55
Feature _{CW}	89.98	59.63	54.53	50.62	47.01

Table 1: Classification accuracy (in %) for PGD attack with different maximum perturbations.

3.2 Adversarial Attacks on the CIFAR-10 Dataset

In this section we consider three different classifiers for CIFAR-10, trained to be robust against adversarial attacks: (i) Madry defense: a Wide-Resnet 32-10-based model of Madry et al. [2018] trained by adversarial training with 7-step PGD attack with $\epsilon = \frac{8}{255}$.² (ii) Free adversarial training: a recently proposed training scheme by Shafahi et al. [2019] which performs the adversarial training without incurring the extra cost used for generating adversarial images by Madry et al. [2018], using the same Wide-Resnet 32-10 as Madry defense; we refer to this defense scheme as Free defense³. (iii) Feature scattering: the recent feature-scattering-based adversarially trained model of Zhang and Wang [2019] using a Wide-ResNet 28-10 model of Zagoruyko and Komodakis [2016], referred to as Feature defense⁴.

All three of these defense schemes have been shown to be robust against the 20-step PGD attack when the attack uses either the standard cross-entropy-loss (xent) or the Carlini-Wagner loss (CW) [Carlini and Wagner, 2017] (given in Eq. 1 with $c = 1$ and $\mathcal{K} = 0$) in the optimization to find an adversarial example. We then consider the performance of these adversarially trained networks when the perturbation ϵ used in a 20-step PGD attack increases beyond the standard $\frac{8}{255}$ used in evaluating these defense schemes in the literature. Analyzing the quality of the produced adversarial images, we first demonstrate (similarly to our experiments on MNIST) that using L_p norms to quantify the quality of the adversarial images can be quite misleading, giving hard-to-interpret accuracy results when the perceptual quality of these adversarial examples are not considered. The classification accuracy on the adversarially perturbed test sets with different perturbation limits ϵ (including the clean test set accuracy with $\epsilon = 0$) is shown in Table 1 (the classifiers are denoted by the name of the model, Madry, Free, or Feature, with a subscript referring to the loss).

Table 1 shows that both Madry defense and Free defense break down as soon as the perturbation size is increased

²We use the pretrained model from the repository provided by Madry et al. [2018].

³We train a robust model using the code provided with the paper Shafahi et al. [2019].

⁴We use the pretrained model from the repository provided by Zhang and Wang [2019].

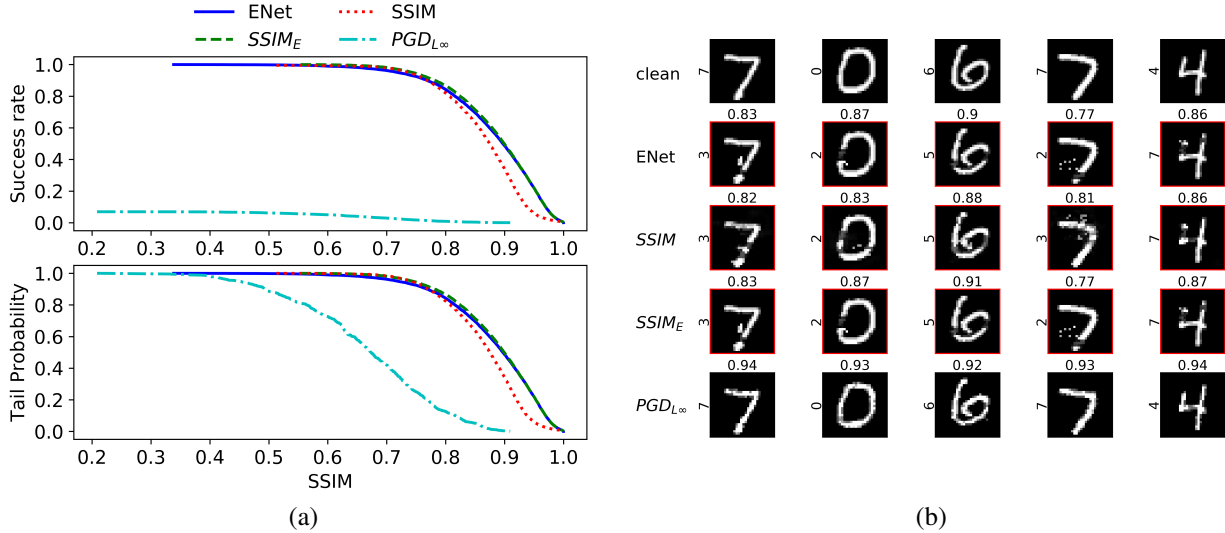


Figure 4: (a) Success rate and proportion of adversarial images as a function of the minimum required SSIM value for adversarial attacks on the MNIST dataset. (b) Adversarial images for the SSIM attack with SSIM values of at least 0.8.

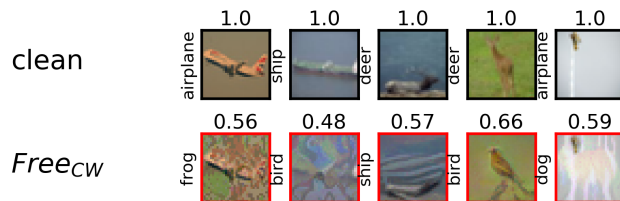


Figure 5: CIFAR-10 dataset: Low-quality adversarial images for the PGD attack and Free defense.

beyond $\epsilon = \frac{8}{255}$, which is used in the training of these networks. Feature defense is the most robust among our models, achieving non-trivial accuracy even for large values of ϵ .

However, inspecting the actual adversarial images used in the attacks, it can be observed that in many cases the image has been either destroyed beyond recognition or modified to represent another class. As an illustration, Figure 5 shows images with low SSIM values (from all the attacks) for $\epsilon = \frac{20}{255}$ (images for more defense schemes are shown in Figure 8(a) in the appendix). For example, it can be seen that for the Free defense with CW attack, clean images of airplane and deer now indeed contain images of a frog, a dog and a bird. Hence, the reduced classification accuracy at larger perturbations for the PGD attack does not represent the true robustness of these networks (interestingly, as demonstrated in Figure 8(a), Feature defense maintains higher accuracy for these modified images with larger perturbations than Free or Madry).

To improve the perceptual quality of the 20-step PGD attack, we can select a successful adversarial image from all the steps with the highest SSIM value, which we call the *SSIM-filtered* attack (this can be applied to other iterative attacks). A higher SSIM value typically provides an image with better quality, as demonstrated by randomly selected examples for the Feature defense with PGD attack and CW-loss in Figure 9 in the appendix. These images also indicate (which can be observed more generally) that an SSIM value of about 0.7 is sufficient to have recognizable image classes. Figure 8(b) in the appendix shows adversarial images with the smallest SSIM values above 0.7; comparing with Figure 8(a) demonstrates that this simple SSIM-filtering can significantly improve the perceptual quality of the resulting adversarial images.

Figure 6 shows the success rate of this SSIM-filtered PGD attack against the different defense schemes (trained with xent and CW loss) as a function of the minimum required SSIM value, compared to the original attacks where the SSIM value of the last step is used (the proportion of the adversarial images with at least the given SSIM value is

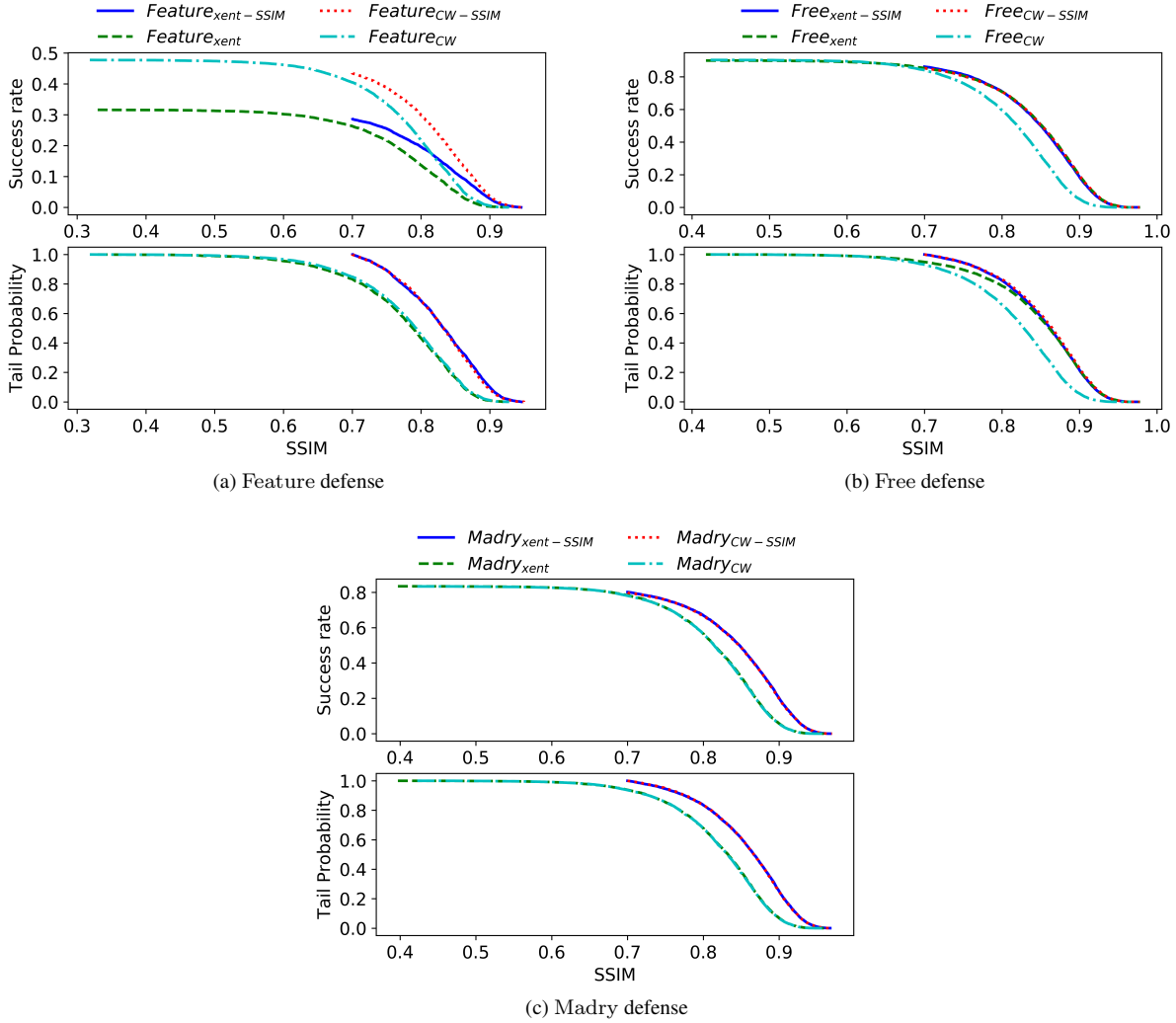


Figure 6: CIFAR-10 dataset: Attack success rate comparison for PGD-attack and SSIM-filtered PGD-attack.

also shown). It can be seen that using SSIM-filtering in the attack results in adversarial images with improved SSIM values, for example, when the SSIM of a successful adversarial example is constrained to be at least 0.8, there is about a 6-11% increase in the attack success rate for all defense schemes for the SSIM-filtered attack. Furthermore, comparing the results to Table 1, one can observe that the attack successes for an SSIM constraint of at least 0.7 are only slightly deteriorated and almost achieve the same success rate as if we do not filter for the SSIM values. The graphs also demonstrate that the PGD attack can achieve high success rate against the considered defense schemes even if we require relatively high quality adversarial images.

Next we evaluate the robustness of the Madry, Free, and Feature defense schemes against our stronger attacks, ENet, SSIM, and SSIM_E, which produce adversarial perturbations not limited by any L_p -norm. ENet is used with the same parameters as for MNIST. For SSIM and SSIM_E, all parameters are the same as for MNIST, except for the thresholds ζ_1 and ζ_2 , which are chosen to be 0.99, as the SSIM values are relatively higher for CIFAR-10 even for larger perturbations (this is due to the averaging of SSIM over the different color channels).⁵ The achieved accuracy, average distortions, and success rate are shown in Figure 7 (in the figure, the name of the attack method is added as a

⁵To save on computation (as the networks are quite large), these experiments were run on 1000 images from the CIFAR-10 test set.

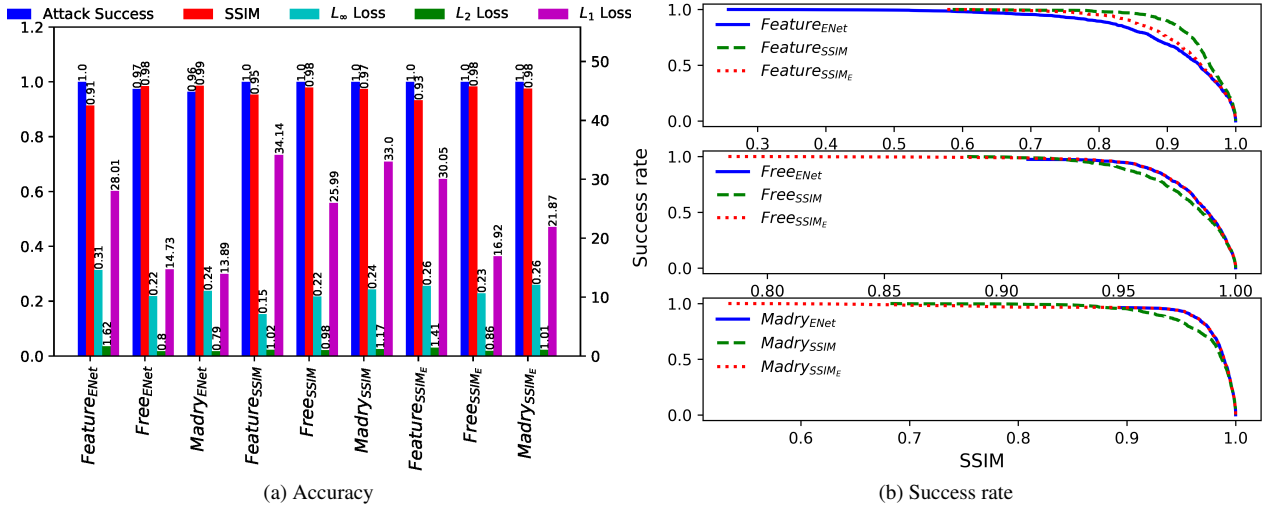


Figure 7: CIFAR-10 dataset: Accuracy and attack success rate comparison for the ENet, SSIM, and SSIM_E attacks.

subscript to the name of the defense scheme). We can see that the SSIM values on average are very high for all attacks. On the other hand, the successful attacks sometimes introduce some artifacts in the images, which are clearly visible (see Figure 10 in the appendix), although typically do not interfere with the class of the new images. It can be seen that for Feature defense (the strongest defense against the PGD attack), the ENet attack results in a large number of adversarial images having SSIM below 0.7, which accounts for 4.5% of all successful adversarial images. In contrast, for SSIM only 0.65% of the successful adversarial images have SSIM below 0.7. Perhaps surprisingly, the ENet attack is unable to achieve 100% adversarial success rate against the Free and Madry defenses, but the SSIM and SSIM_E attacks achieve 100% adversarial success rate against all defense schemes when no constraint is imposed on the SSIM value. One can also see that the SSIM attack (and also SSIM_E) provides a significant improvement in the SSIM values of the successful adversarial examples compared to ENet, especially for the most effective defense scheme, Feature. For example, at an SSIM level of 0.8, the SSIM attack achieves a 10% higher success rate than ENet, which goes up to 20% when the SSIM is 0.9 (which accounts for an almost 30% relative improvement). Figure 10 in the appendix shows the successful adversarial images for the ENet attack with the lowest SSIM values for the Feature defense, which are nearly destroyed, while the corresponding adversarial images obtained by SSIM and SSIM_E have high SSIM values and are perceptually very similar to the original images. For a fair comparison, Figure 11 in the appendix shows the successful adversarial images for the SSIM attack with the lowest SSIM values for the Feature defense, which are not destroyed beyond recognition. Visually inspecting the adversarial images from the attacks for different SSIM values of at least 0.7, as shown in Figure 12 in the appendix, it can be seen that even for very high values of SSIM (at least 0.95) modifications are not truly imperceptible.

Hence, it can be concluded that even though the state-of-the-art Madry, Free and Feature defense schemes achieve robustness against bounded adversarial perturbations, their performance deteriorates quickly as soon as the size of the perturbations increase even for the PGD attack. In order to keep these potentially unbounded perturbations perceptually similar to the original images, we can use SSIM to disallow images of too low quality. Allowing only images with an SSIM value of at least 0.7, the attacks achieve similar performance as the unbounded attacks but with better perceptual quality. Compared to the Madry and Free defense schemes, Feature defense is the most robust against these unbounded perturbations produced using the PGD attack, but the more advanced optimization-based attacks (ENet, SSIM and SSIM_E) also break this defense completely even though the successful adversarial images, especially for SSIM and SSIM_E, are perceptually very similar to the original ones. This highlights the shortcomings of current measures for the evaluation of robustness of defense schemes against bounded adversarial perturbations, and justifies the use of perception-based attacks, such as our proposed SSIM-based methods.

4 Conclusions

In this paper, we proposed to use the perceptual similarity measure SSIM as the quality metric instead of standard L_p -distances for both adversarial attacks and evaluating the robustness of adversarial defense schemes. Experiments on the MNIST and the CIFAR-10 datasets demonstrate that our proposed adversarial attacks (SSIM and SSIM_E) achieve the same or higher success rate as state-of-the-art attacks using possibly unbounded perturbations (such as the elastic net attack), while producing adversarial images of better perceptual quality. Our experiments also demonstrate that it is possible to completely break recent state-of-the-art defense schemes (such as the feature-scattering defense) with adversarial examples of high perceptual quality.

References

- Anish Athalye, Nicholas Carlini, and David Wagner. Obfuscated gradients give a false sense of security: Circumventing defenses to adversarial examples. In *International Conference on Machine Learning*, pages 274–283, 2018.
- Joan Bruna, Christian Szegedy, Ilya Sutskever, Ian Goodfellow, Wojciech Zaremba, Rob Fergus, and Dumitru Erhan. Intriguing properties of neural networks. In *International Conference on Learning Representations*, 2014.
- Dominique Brunet, Edward R Vrscay, and Zhou Wang. On the mathematical properties of the structural similarity index. *IEEE Transactions on Image Processing*, 21(4):1488–1499, 2011.
- Nicholas Carlini and David Wagner. Towards evaluating the robustness of neural networks. In *2017 IEEE Symposium on Security and Privacy (SP)*, pages 39–57. IEEE, 2017.
- Yair Carmon, Aditi Raghunathan, Ludwig Schmidt, John C Duchi, and Percy S Liang. Unlabeled data improves adversarial robustness. In *Advances in Neural Information Processing Systems*, pages 11190–11201, 2019.
- Pin-Yu Chen, Yash Sharma, Huan Zhang, Jinfeng Yi, and Cho-Jui Hsieh. Ead: elastic-net attacks to deep neural networks via adversarial examples. In *Thirty-Second AAAI Conference on Artificial Intelligence*, 2018.
- Jeremy Cohen, Elan Rosenfeld, and Zico Kolter. Certified adversarial robustness via randomized smoothing. In *International Conference on Machine Learning*, pages 1310–1320, 2019.
- Andrew Cotter, Heinrich Jiang, and Karthik Sridharan. Two-player games for efficient non-convex constrained optimization. In *Algorithmic Learning Theory*, pages 300–332, 2019.
- Gintare Karolina Dziugaite, Zoubin Ghahramani, and Daniel M Roy. A study of the effect of jpg compression on adversarial images. *arXiv preprint arXiv:1608.00853*, 2016.
- Ian J Goodfellow, Jonathon Shlens, and Christian Szegedy. Explaining and harnessing adversarial examples. In *International Conference on Learning Representations*, 2015.
- Sven Gowal, Krishnamurthy Dvijotham, Robert Stanforth, Rudy Bunel, Chongli Qin, Jonathan Uesato, Timothy Mann, and Pushmeet Kohli. On the effectiveness of interval bound propagation for training verifiably robust models. *arXiv preprint arXiv:1810.12715*, 2018.
- Diego Gragnaniello, Francesco Marra, Giovanni Poggi, and Luisa Verdoliva. Perceptual quality-preserving black-box attack against deep learning image classifiers. *arXiv preprint arXiv:1902.07776*, 2019.
- Chuan Guo, Mayank Rana, Moustapha Cisse, and Laurens van der Maaten. Countering adversarial images using input transformations. In *International Conference on Learning Representations*, 2018.
- Ruitong Huang, Bing Xu, Dale Schuurmans, and Cs. Szepesvari. Learning with a strong adversary. *ArXiv*, abs/1511.03034, 2015.

- Diederik P Kingma and Jimmy Ba. Adam: A method for stochastic optimization. In *International Conference on Learning Representations*, 2015.
- Alex Krizhevsky. Learning multiple layers of features from tiny images. Technical report, University of Toronto, 2009.
- Alexey Kurakin, Ian Goodfellow, and Samy Bengio. Adversarial machine learning at scale. In *International Conference on Learning Representations*, 2017.
- Yann LeCun and Corinna Cortes. MNIST handwritten digit database. <http://yann.lecun.com/exdb/mnist/>, 2010.
- Aleksander Madry, Aleksandar Makelov, Ludwig Schmidt, Dimitris Tsipras, and Adrian Vladu. Towards deep learning models resistant to adversarial attacks. In *International Conference on Learning Representations*, 2018.
- Nicolas Papernot, Fartash Faghri, Nicholas Carlini, Ian Goodfellow, Reuben Feinman, Alexey Kurakin, Cihang Xie, Yash Sharma, Tom Brown, Aurko Roy, Alexander Matyasko, Vahid Behzadan, Karen Hambardzumyan, Zhishuai Zhang, Yi-Lin Juang, Zhi Li, Ryan Sheatsley, Abhibhav Garg, Jonathan Uesato, Willi Gierke, Yinpeng Dong, David Berthelot, Paul Hendricks, Jonas Rauber, and Rujun Long. Technical report on the cleverhans v2.1.0 adversarial examples library. *arXiv preprint arXiv:1610.00768*, 2018.
- Nicolas Papernot *et al.* Practical black-box attacks against machine learning. In *ACM Asia Conf. Comp. and Comm. Security*, pages 506–519, 2017.
- Jérôme Rony, Luiz G Hafemann, Luiz S Oliveira, Ismail Ben Ayed, Robert Sabourin, and Eric Granger. Decoupling direction and norm for efficient gradient-based l2 adversarial attacks and defenses. In *Proceedings of the IEEE Conference on Computer Vision and Pattern Recognition*, pages 4322–4330, 2019.
- Ali Shafahi, Mahyar Najibi, Mohammad Amin Ghiasi, Zheng Xu, John Dickerson, Christoph Studer, Larry S Davis, Gavin Taylor, and Tom Goldstein. Adversarial training for free! In *Advances in Neural Information Processing Systems*, pages 3353–3364, 2019.
- Mahmood Sharif, Lujo Bauer, and Michael K Reiter. On the suitability of l_p -norms for creating and preventing adversarial examples. In *Proceedings of the IEEE Conference on Computer Vision and Pattern Recognition Workshops*, pages 1605–1613, 2018.
- Florian Tramèr, Alexey Kurakin, Nicolas Papernot, Ian Goodfellow, Dan Boneh, and Patrick McDaniel. Ensemble adversarial training: Attacks and defenses. In *International Conference on Learning Representations*, 2018.
- Zhou Wang and Alan C Bovik. A universal image quality index. *IEEE Signal Processing Letters*, 9(3):81–84, 2002.
- Zhou Wang, Alan C Bovik, Hamid R Sheikh, and Eero P Simoncelli. Image quality assessment: from error visibility to structural similarity. *IEEE transactions on image processing*, 13(4):600–612, 2004.
- Weilin Xu, David Evans, and Yanjun Qi. Feature squeezing: Detecting adversarial examples in deep neural networks. In *Network and Distributed Systems Security Symposium (NDSS) 2018*, 2018.
- Ziang Yan, Yiwen Guo, and Changshui Zhang. Deep defense: Training dnns with improved adversarial robustness. In *Advances in Neural Information Processing Systems*, pages 417–426, 2018.
- Hector Yee, Sumanita Pattanaik, and Donald P Greenberg. Spatiotemporal sensitivity and visual attention for efficient rendering of dynamic environments. *ACM Transactions on Graphics (TOG)*, 20(1):39–65, 2001.
- Sergey Zagoruyko and Nikos Komodakis. Wide residual networks. In *Proceedings of the British Machine Vision Conference (BMVC)*, pages 87.1–87.12. BMVA Press, September 2016.
- Haichao Zhang and Jianyu Wang. Defense against adversarial attacks using feature scattering-based adversarial training. In *Advances in Neural Information Processing Systems*, 2019.
- Zhengyu Zhao, Zhuoran Liu, and Martha Larson. Towards large yet imperceptible adversarial image perturbations with perceptual color distance. In *Proceedings of the IEEE/CVF Conference on Computer Vision and Pattern Recognition*, pages 1039–1048, 2020.

APPENDIX

A Binary search algorithm to set c in (1)

The binary search algorithm to tune c in the loss function (1), as proposed by Chen et al. [2018] for the ENet attack, is shown in Algorithm 2. In the experiments we ran the search for $K = 9$ steps.

Algorithm 2 Binary search algorithm for parameter c in (1).

Input: $K \in \mathbb{N}$, $c_{init} = 10^{-3}$, classifier f , adversarial attack A , quality measure Q

Initialize: $c = c_{init}$, LowerBound = 0, UpperBound = 10^{10}

for $k \in K$ **do**

$x + \delta = A(c, x)$

$\hat{s} = f(x + \delta)$, $s = f(x)$

if $\hat{s} \neq s$ **then**

 UpperBound = $\min(\text{UpperBound}, c)$

if UpperBound < 10^9 **then**

$c = \frac{\text{LowerBound} + \text{UpperBound}}{2}$

end if

else

 LowerBound = $\max(\text{LowerBound}, c)$

if UpperBound < 10^9 **then**

$c = \frac{\text{LowerBound} + \text{UpperBound}}{2}$

else

$c = 10c$

end if

end if

end for

Return $x + \delta$ with highest quality measure Q found in the K iterations.

B Additional images

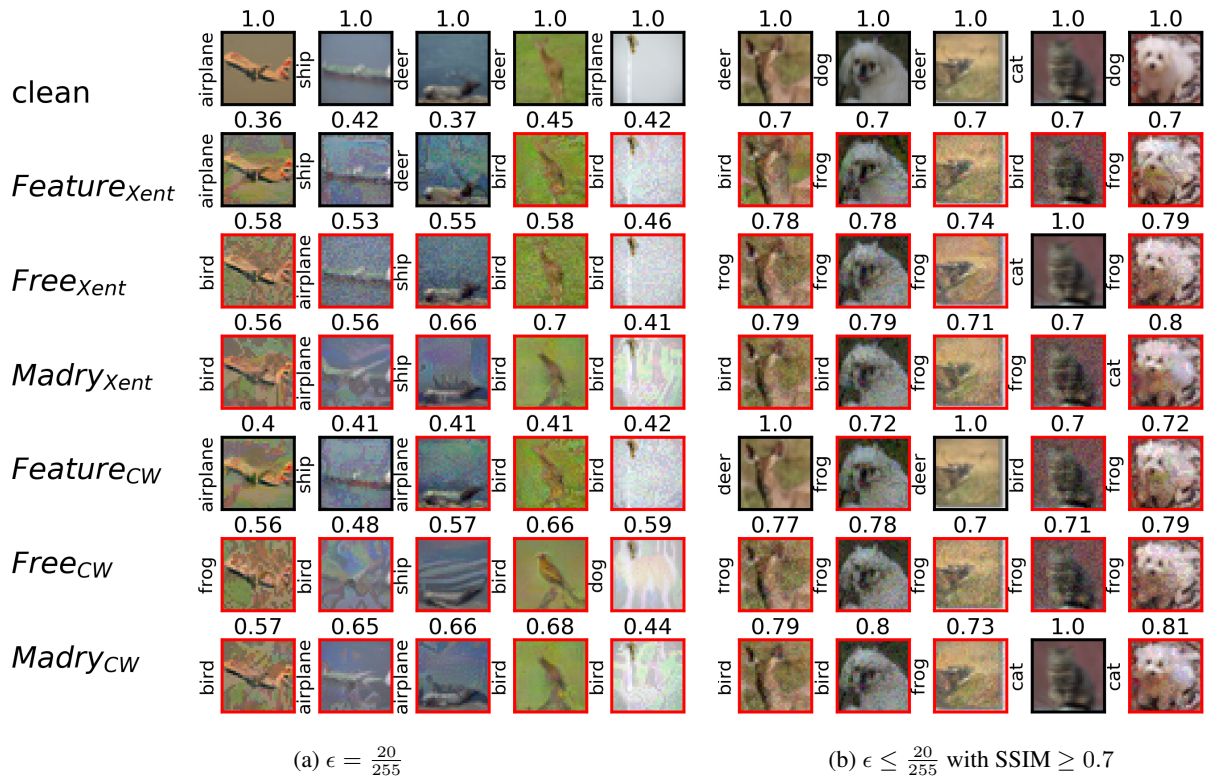


Figure 8: CIFAR-10 dataset: Adversarial images for PGD attack.

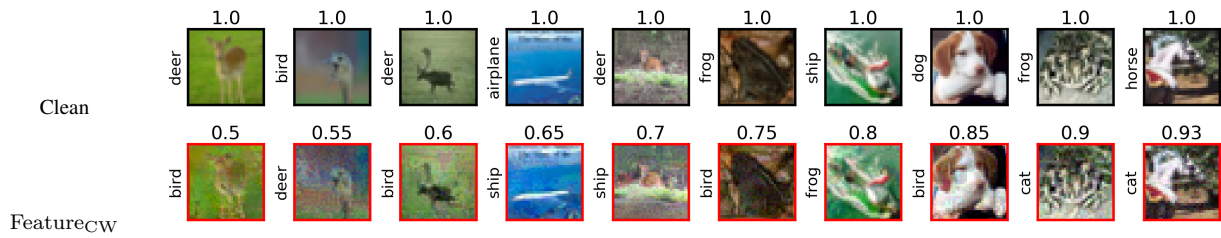


Figure 9: CIFAR-10 dataset: Adversarial images for perturbation $\epsilon = \frac{20}{255}$.



Figure 10: CIFAR-10 dataset: Adversarial images produced by the ENet attack with lowest SSIM values.

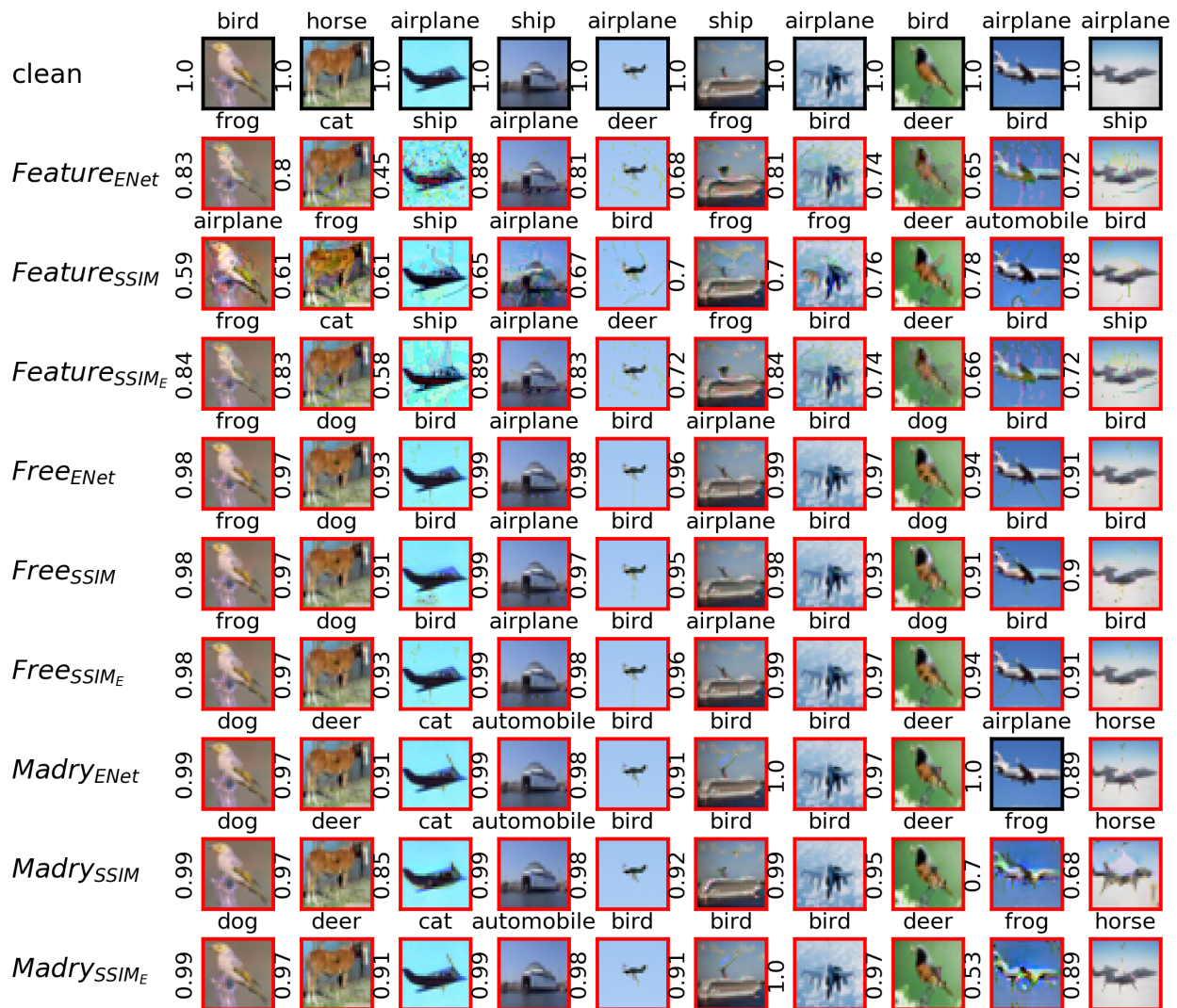
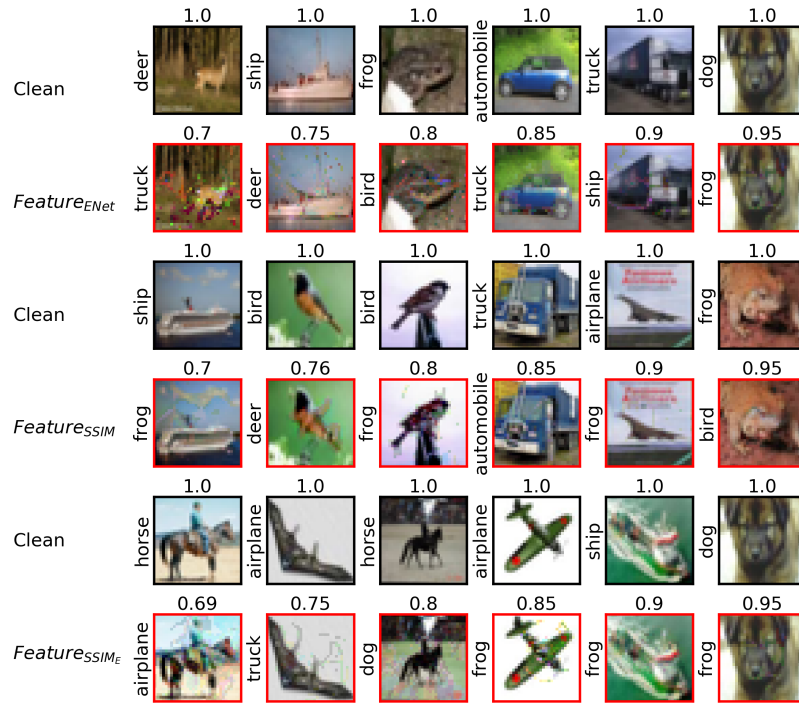
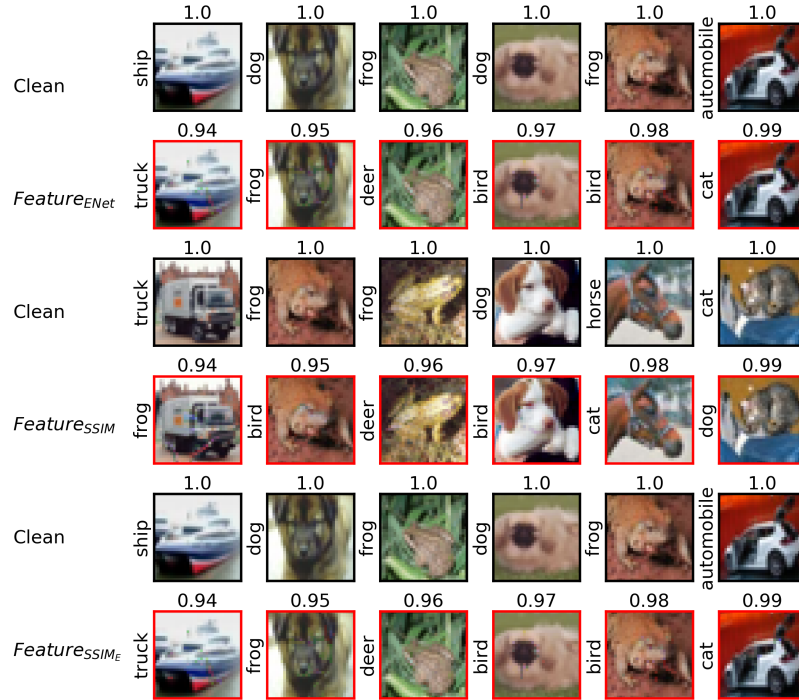


Figure 11: CIFAR-10 dataset: Adversarial images produced by the SSIM attack with lowest SSIM values.



(a)



(b)

Figure 12: CIFAR-10 dataset: Adversarial images for ENet, SSIM and $SSIM_E$ -attack with different SSIM values: (a) low SSIM values; (b) high SSIM values (the attack is shown as the subscript to the name of the defense method).